Article

Cell Reports

A Vitamin D Receptor Selectively Activated by Gemini Analogs Reveals Ligand Dependent and Independent Effects

Graphical Abstract

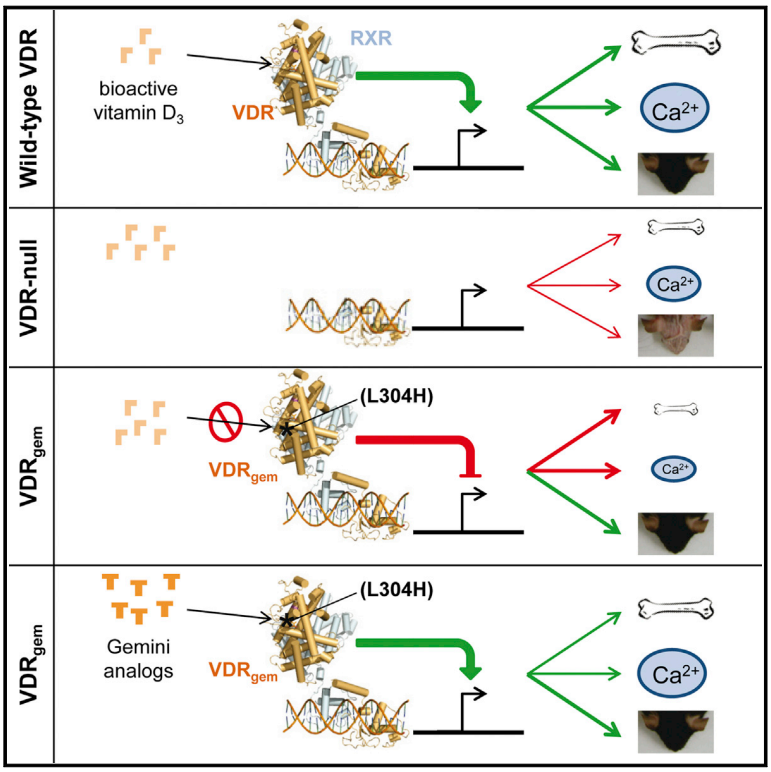

Authors

Tiphaine Huet, Gilles Laverny, ..., Dino Moras, Natacha Rochel

Correspondence

metzger@igbmc.fr (D.M.), rochel@igbmc.fr (N.R.)

In Brief

Mutant mice expressing a vitamin D receptor (VDR) that is unresponsive to its natural ligand reveals that signaling through the VDR can be ligand dependent or independent. The two pathways have different impacts in mineral and bone homeostasis.

Highlights

- A point-mutated VDR (VDR_{gem}) is selectively activated by gemini ligands
- Skeletal defects are more severe in VDR_{gem} mice than in VDR null mice
- VDR_{gem} represses VDR target genes
- Transcriptional activity of VDR_{gem} is restored in mice by gemini ligands

Accession Numbers

4RUJ
4RUO
4RUP

Huet et al., 2015, Cell Reports *10*, 516–526
February 3, 2015
http://dx.doi.org/10.1016/j.celrep.2014.12.045

OPEN ACCESS
CellPress

Cell Reports
Article

A Vitamin D Receptor Selectively Activated by Gemini Analogs Reveals Ligand Dependent and Independent Effects

Tiphaine Huet,[1,4,6] Gilles Laverny,[2,4] Fabrice Ciesielski,[1,7] Ferdinand Molnár,[1,8] Thanuja Gali Ramamoorthy,[2,9] Anna Y. Belorusova,[1] Pierre Antony,[1] Noelle Potier,[3] Daniel Metzger,[2,5,*] Dino Moras,[1,5] and Natacha Rochel[1,5,*]

[1]Department of Integrative Structural Biology, Institut de Génétique et de Biologie Moléculaire et Cellulaire (IGBMC), Institut National de la Santé et de la Recherche Médicale (INSERM) U964, Centre National de la Recherche Scientifique (CNRS) UMR 7104, Université de Strasbourg, 67404 Illkirch, France

[2]Department of Functional Genomics and Cancer, Institut de Génétique et de Biologie Moléculaire et Cellulaire (IGBMC), Institut National de la Santé et de la Recherche Médicale (INSERM) U964, Centre National de la Recherche Scientifique (CNRS) UMR 7104, Université de Strasbourg, 67404 Illkirch, France

[3]Institut de Chimie LC3-CNRS-UMR 7177, 67008 Strasbourg, France

[4]Co-first author

[5]Co-senior author

[6]Present address: CBS, Montpellier, France

[7]Present address: Novalix, 67405 Illkirch, France

[8]Present address: Institute of Biopharmacy, School of Pharmacy, University of Eastern Finland, 70211 Kuopio, Finland

[9]Present address: Faculty of Life Sciences, University of Manchester, Manchester M13 9PL, UK

*Correspondence: metzger@igbmc.fr (D.M.), rochel@igbmc.fr (N.R.)

http://dx.doi.org/10.1016/j.celrep.2014.12.045

SUMMARY

The bioactive form of vitamin D [1,25(OH)$_2$D$_3$] regulates mineral and bone homeostasis and exerts potent anti-inflammatory and antiproliferative properties through binding to the vitamin D receptor (VDR). The 3D structures of the VDR ligand-binding domain with 1,25(OH)$_2$D$_3$ or gemini analogs unveiled the molecular mechanism underlying ligand recognition. On the basis of structure-function correlations, we generated a point-mutated VDR (VDR$_{gem}$) that is unresponsive to 1,25(OH)$_2$D$_3$, but the activity of which is efficiently induced by the gemini ligands. Moreover, we show that many VDR target genes are repressed by unliganded VDR$_{gem}$ and that mineral ion and bone homeostasis are more impaired in VDR$_{gem}$ mice than in VDR null mice, demonstrating that mutations abolishing VDR ligand binding result in more severe skeletal defects than VDR null mutations. As gemini ligands induce VDR$_{gem}$ transcriptional activity in mice and normalize their serum calcium levels, VDR$_{gem}$ is a powerful tool to further unravel both liganded and unliganded VDR signaling.

INTRODUCTION

The active form of vitamin D, 1α,25-dihydroxyvitamin D3 [1,25(OH)$_2$D$_3$], plays a key role in mineral and bone homeostasis (Bouillon et al., 2008; Bouillon and Suda, 2014; Lieben and Carmeliet, 2013b). Indeed, 1,25(OH)$_2$D$_3$ deficiency induced by low sunlight exposure or the lack of functional 25(OH)-vitaminD$_3$-1α-hydroxylase (Cyp27b1), the enzyme that catalyzes the hydroxylation of 25(OH)D$_3$ to 1,25(OH)$_2$D$_3$, in pseudovitamin D-deficiency rickets (PDRR, also termed vitamin D-dependent rickets type I [VDRR-I]), induces skeletal deformities, osteomalacia, hypocalcemia, hypophosphatemia, and secondary hyperparathyroidism, which can be treated by 1,25(OH)$_2$D$_3$ or analogs (Dardenne et al., 2001, 2003; Lips, 2006; Panda et al., 2001). 1,25(OH)$_2$D$_3$, through binding to the vitamin D receptor (VDR; NR1I1), a member of the nuclear receptor superfamily, regulates the expression of many target genes in various tissues (Bouillon et al., 2008). VDR loss-of-function mutations in humans, termed hereditary vitamin D-resistant rickets (HVDRRs) or VDDR-II, and VDR-null mice exhibit typical hallmarks of rickets (Li et al., 1997; Malloy et al., 2014; Yoshizawa et al., 1997). In contrast to Cyp27b1 null mice and patients expressing a mutated VDR with reduced affinity for 1,25(OH)$_2$D$_3$, VDR DNA-binding-deficient patients and VDR-null mice exhibit alopecia. Hair follicle defects in VDR null mice are prevented by transgenic expression of full-length or ligand-binding-deficient VDR in keratinocytes (Skorija et al., 2005). Thus, whereas liganded VDR is essential for mineral and bone homeostasis, ligand-independent functions of VDR maintain hair follicle homeostasis (Chen et al., 2001; Lieben et al., 2011; Malloy and Feldman, 2011; Skorija et al., 2005). 1,25(OH)$_2$D$_3$ also has potent anti-inflammatory and antiproliferative properties and is thus a potential pharmacological agent to treat various diseases, including autoimmune disorders, infections, and cancer (Adorini et al., 2007). Nevertheless, the 1,25(OH)$_2$D$_3$ doses required to elicit such effects induce hypercalcemia, resulting in ectopic calcification of the vascular wall, kidney, and other soft tissues, leading to organ failure and death (Adorini et al., 2007; Bouillon et al., 2008).

In order to dissociate the calcemic activities of $1,25(OH)_2D_3$ from its anti-inflammatory and antiproliferative properties, more than 3,000 analogs were synthesized using medicinal chemistry approaches (Adorini et al., 2007; Laverny et al., 2009; Leyssens et al., 2014). Even though the resolution of the VDR ligand binding domain (LBD) 3D structure facilitates the design of VDR agonists, no potent antiproliferative and/or anti-inflammatory compounds devoid of hypercalcemic activities have been obtained (Laverny et al., 2009; Lee et al., 2008). Furthermore, available mouse lines in which $1,25(OH)_2D_3$ or VDR signaling is impaired exhibit limitations for identifying tissue-specific ligand-dependent and ligand-independent VDR activities. Indeed, all VDR-mediated effects are abolished in various organs of VDR null mice, and compensatory mechanisms occur in tissue-specific VDR null mice (Lieben and Carmeliet, 2013a; Lieben et al., 2012; Yoshizawa et al., 1997). In addition, increased circulating levels of the low-affinity VDR ligand $25(OH)D_3$ in $1,25(OH)_2D_3$-deficient Cyp27b1 null mice might partially induce VDR target genes (Lou et al., 2010; Panda et al., 2001).

Among the various synthetic vitamin D analogs, the gemini family is characterized by an additional aliphatic side chain. These ligands induce specific conformational changes in the *Danio rerio* VDR ligand binding pocket (LBP), including a reorientation of the side chain of Leu337, the second N-terminal Leu of helix 7, which opens a pocket that accommodates the second side chain of such ligands (Ciesielski et al., 2007; Huet et al., 2011). We previously showed that the substitution of the corresponding amino acid in human VDR (Leu309) with hydrophobic residues (Met and Phe) had little or no effect on $1,25(OH)_2D_3$- and gemini-induced transcriptional activity (Ciesielski et al., 2007).

In the present study, we report that substitution of the second N-terminal Leu residue of VDR helix 7 with the hydrophilic residue His (VDR_{gem}) impairs binding of $1,25(OH)_2D_3$, but not of the gemini synthetic analogs and reveal the underlying molecular mechanisms. Based on the unique characteristics of this receptor variant, we generated mice bearing this substitution to evaluate the in vivo role of unliganded and liganded VDR and further characterize VDR signaling.

RESULTS

Substitution of zVDR Leucine 337 or hVDR Leucine 309 by a Histidine Impairs Binding of $1,25(OH)_2D_3$ but Not of Gemini

With the aim to impair $1,25(OH)_2D_3$ binding to its receptor without affecting binding of gemini analogs, we substituted the *Danio rerio* VDR (zVDR) Leu337 by a hydrophilic His residue ($zVDR_{gem}$) (Figures 1A and 1B) and analyzed the functional consequences. In vitro binding of $1,25(OH)_2D_3$ or gemini [1,25-dihydroxy-21-(3-hydroxy-3-methylbutyl)-vitamin D_3] was monitored by electrospray-ionization mass spectrometry (ESI-MS) under nondenaturating conditions using purified bacterially-produced LBDs of zVDR and $zVDR_{gem}$. In the presence of a 5-fold molar excess of $1,25(OH)_2D_3$ or gemini, more than 90% of the zVDR LBDs bind the ligand at a 1:1 ratio (Figure S1). Under similar ligand concentrations, 90% of the $zVDR_{gem}$ LBDs bind gemini, whereas only 10% are liganded with $1,25(OH)_2D_3$ (Figures 1C and 1D). The capillary voltages at which 50% of the complexes are dissociated (VC50) for zVDR-$1,25(OH)_2D_3$, zVDR-gemini, and $zVDR_{gem}$-gemini are in the same range (i.e., 149, 153, and 152 V, respectively), indicating a similar binding affinity of both ligands for zVDR and of the gemini ligand for both receptors (Table S1). In contrast, the 90% of $zVDR_{gem}$ detected in presence of $1,25(OH)_2D_3$ correspond to those of the unliganded receptor (Figure 1C). Consequently, the corresponding VC50 could not be determined. Similar results were obtained by substituting the human VDR Leu309 by a His ($hVDR_{gem}$) (Figure S2; Table S1A). Thus, in contrast to VDR, VDR_{gem} exhibits a strong binding preference for gemini over $1,25(OH)_2D_3$.

To characterize the molecular mechanisms underlying this preferential ligand binding, $zVDR_{gem}$ LBD was crystallized in the presence of 3-fold excess of either $1,25(OH)_2D_3$, gemini or the gemini analog 1,25-dihydroxy-21(3-hydroxy-3-trifluomethyl-4-trifluoro-butynyl)-26,27-hexadeutero-19-nor-20S-vitamin D_3 (BxI-72; Gemini-72) (Huet et al., 2011; Maehr et al., 2007) (Figure 1A) and a steroid receptor coactivator (SRC) peptide encompassing a LXXLL nuclear receptor interacting motif. Although VDR_{gem} has a low affinity for $1,25(OH)_2D_3$, the ligand concentration used for crystallization allows a significant fraction of the $1,25(OH)_2D_3$ bound complex to be crystallized. Crystals formed in presence of $1,25(OH)_2D_3$, gemini, or Gemini-72 are isomorphous and belong to the space group $P6_522$, with one LBD complex per asymmetric unit. The 3D structures were solved by molecular replacement and refined to 2.35, 2.80, and 2.75 Å for $zVDR_{gem}$-$1,25(OH)_2D_3$, $zVDR_{gem}$-gemini, and $zVDR_{gem}$-Gemini-72, respectively (Table S2). All complexes display the canonical agonist conformation (data not shown; Huet et al., 2011; Rochel and Moras, 2006; Rochel et al., 2000). In the $1,25(OH)_2D_3$-liganded zVDR LBD, Gln426 of helix 11 stabilizes His333 of helix 6, which anchors the ligand via a hydrogen bond with the 25-hydroxyl group of $1,25(OH)_2D_3$ (Figure 1E). However, a conformational change occurs in the $1,25(OH)_2D_3$-$zVDR_{gem}$ complex, where the substituted His337 perturbs the orientation of Gln426, thereby preventing its interaction with His333 (Figures 1F and S3A). Consequently, the distances between the 25-hydroxyl group and the two anchoring His residues (His333 and His423) increase from 2.7 and 2.8 Å in the zVDR-$1,25(OH)_2D_3$ complex to 3.1 Å in the $zVDR_{gem}$-$1,25(OH)_2D_3$ complex, thus weakening the corresponding hydrogen bonds. In contrast, the second side chain of the gemini analogs induces a reorientation of His337 that now points toward the solvent, whereas Gln426 is in a similar orientation than in the agonist bound zVDR and interacts with His333 located at a distance of 2.9 Å (Figures 1G and S3). Moreover, His337 forms an additional electrostatic interaction that stabilizes Gln426. Thus, the molecular mechanism of ligand binding discrimination by VDR_{gem} is explained by a disturbed hydrogen bond networks that impairs binding of $1,25(OH)_2D_3$, but not of gemini ligands.

SRC-1 and Drip205 Coactivator Recruitment by VDR_{gem} Is More Efficient in the Presence of Gemini Than of $1,25(OH)_2D_3$

To analyze the functional consequences of the Leu to His substitution, coactivator peptide recruitment by the LBD of zVDR and

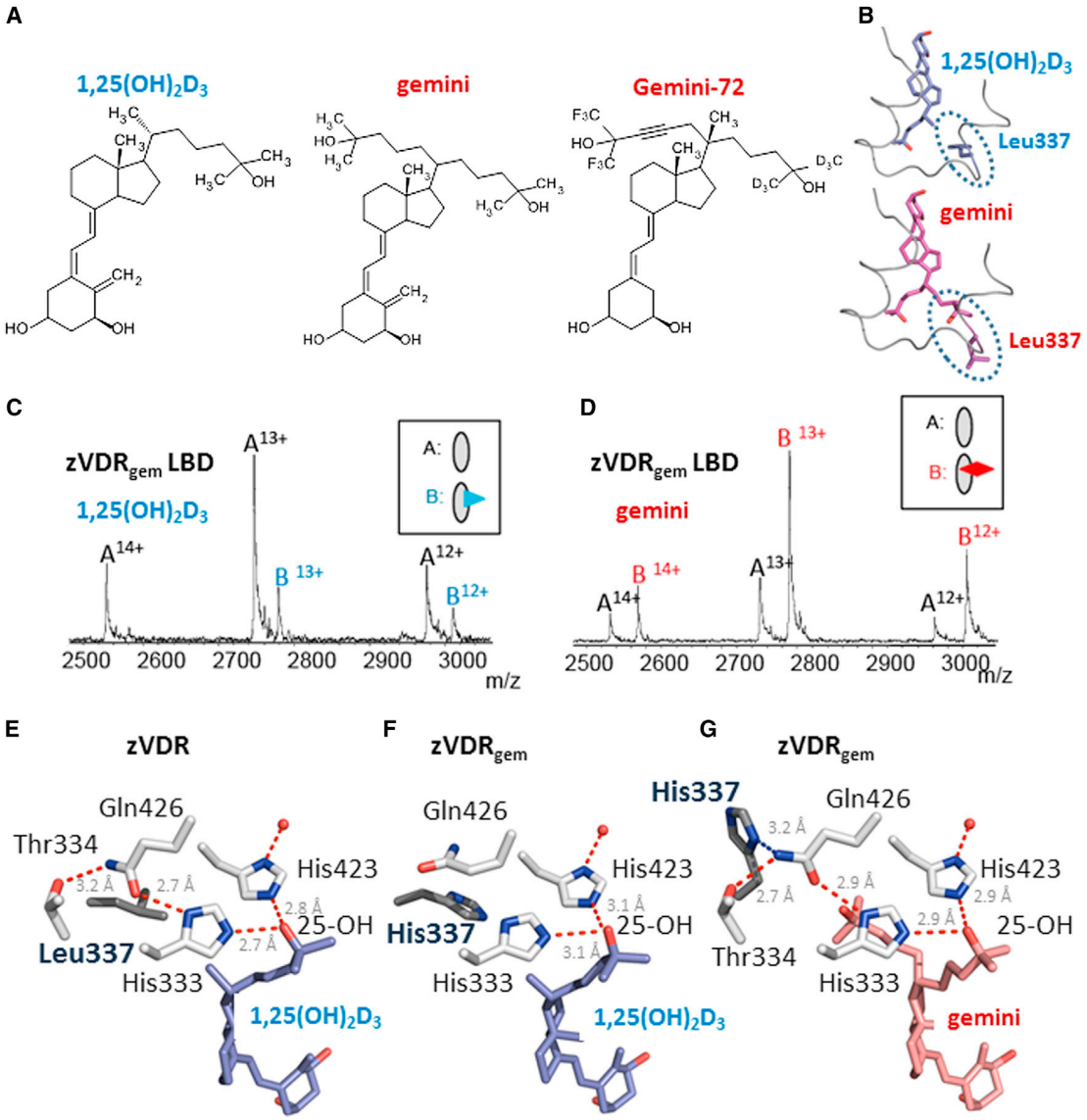

Figure 1. Molecular Mechanism Underlying Selective Binding of Gemini Ligand by zVDR Leu337His

(A) Chemical structures of 1,25(OH)$_2$D$_3$, gemini, and Gemini-72.

(B) Conformational change of Leu337 side chain that opens an additional pocket to fit the second side chain of gemini ligands in the zVDR LBD crystal structure.

(C and D) The substitution of zVDR Leu337 by a His impairs the binding of 1,25(OH)$_2$D$_3$ but not gemini as shown by non-denaturating ESI-MS analysis of ligand binding to zVDR$_{gem}$. Enlarged view of the 12^+, 13^+, and 14^+ ions of the electrospray ionization mass spectrum of zVDR$_{gem}$ LBD in presence of 5-fold molar excess of 1,25(OH)$_2$D$_3$ (blue; C) or gemini (red; D) (see also Figures S1 and S2; Table S1).

(E–G) Detailed views of the structural impact of the mutation in zVDR show the importance of Gln426. In the native zVDR-1,25(OH)$_2$D$_3$ complex, Gln426 interacts with His333 and stabilizes its coordination to the ligand (see also Table S2 and Figure S3) (E). In the zVDR$_{gem}$-1,25(OH)$_2$D$_3$ complex, the mutated residue His337 pushes away Gln426 preventing its interaction with His333 (F). In the complex with gemini, due to the steric effect of the ligand's second side chain, His337 rotates out of the pocket, allowing Gln426 to adopt its WT conformation (G). Moreover, His337 interacts with Gln426 and stabilizes the hydrogen bonds network around the 25-hydroxyl group. The red sphere indicates a conserved water molecule. 1,25(OH)$_2$D$_3$ and gemini are shown in blue and light red, respectively. Nitrogen and oxygen atoms are shown in blue and red, respectively.

zVDR$_{gem}$ was monitored by fluorescence anisotropy in the presence of saturating ligand concentration. Neither LBD in its apo form binds a fluorescently labeled peptide of the SRC-1 coregulator that encompasses one LXXLL nuclear receptor interacting motif (F-SRC-P), whereas in the presence of gemini, zVDR and zVDR$_{gem}$ bind F-SRC-P with a similar affinity (Kd = 3.1 ± 0.2 μM) (Figure S4A; Table S3). In contrast, in the presence of 1,25(OH)$_2$D$_3$, the SRC-1 peptide binding affinity of the zVDR$_{gem}$ LBD is 5.6-fold lower than that of the zVDR LBD (Table S3). Thus, at saturating ligand concentrations, the SRC-1 coactivator

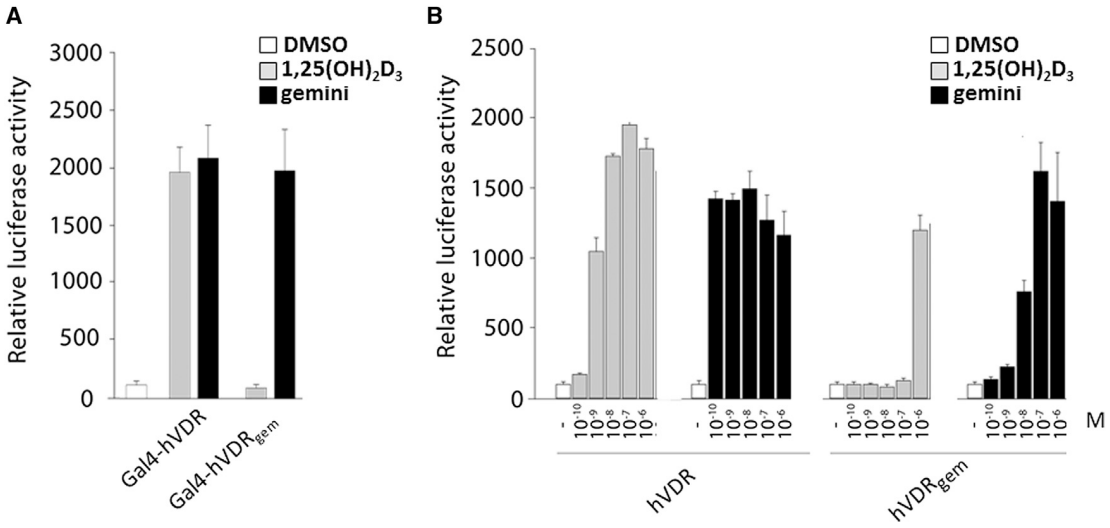

Figure 2. Transcriptional Activities of $hVDR_{gem}$ upon Gemini versus $1,25(OH)_2D_3$ Treatments

(A) Transactivation efficiencies of $hVDR_{gem}$ are severely altered in the presence of $1,25(OH)_2D_3$ but not in the presence of gemini. Transient transfection assays with expression vectors encoding fusion proteins between Gal4 DBD and the LBD of $hVDR_{gem}$ or WT VDR were performed in HEK293 EBNA cells to evaluate their transcriptional activity in response to 100 nM of $1,25(OH)_2D_3$, gemini, or DMSO (vehicle).

(B) Dose-response transcriptional activities of full-length hVDR and $hVDR_{gem}$ on a *CYP24a1* promoter containing luciferase reporter gene were determined in MCF-7 cells. Bars represent the mean ± SD (n = 3) (see also Figure S5).

peptide is efficiently recruited by VDR_{gem} in the presence of gemini, but not in the presence of $1,25(OH)_2D_3$.

The effect of VDR ligands on the interaction between VDR or VDR_{gem} with the coactivators SRC-1 or Drip205 was characterized by a mammalian two-hybrid assay. To this end, HEK293 EBNA cells were cotransfected with expression vectors that encode fusion proteins between either VDR or VDR_{gem} and the viral transactivator VP16 (VDR-VP16 and VDR_{gem}-VP16, respectively) and between the Gal4 DNA binding domain (DBD) and the nuclear receptor interacting domain (NRID) of the coactivators SRC-1 or Drip205 (Gal4-SRC-1 NRID and Gal4-Drip NRID, respectively) and a Gal4 luciferase reporter plasmid. A strong reporter activity is induced by addition of 10 nM $1,25(OH)_2D_3$ to cells expressing either Gal4-SRC-1 NRID or Gal4-Drip NRID in presence of VDR-VP16, but not of VDR_{gem}-VP16. In contrast, a similar reporter activity is observed in such cells treated with 10 nM Gemini-72 (Figure S4B). Thus, whereas both $1,25(OH)_2D_3$ and Gemini-72 efficiently stimulate the recruitment of coactivators to VDR, only the latter promotes their recruitment to VDR_{gem}.

VDR_{gem} Transcriptional Activity Is Selectively and Efficiently Induced by Gemini Ligands

We further characterized the transcriptional activity of VDR_{gem} LBD in HEK293 EBNA cells in the presence of $1,25(OH)_2D_3$ or of gemini analogs. Whereas the transcriptional activities of fusion proteins between the Gal4 DBD and the LBD of either $hVDR_{gem}$ or hVDR (Gal4-$hVDR_{gem}$ and Gal4-hVDR, respectively) are similar in the presence of 100 nM gemini, no transcriptional activity was observed for Gal4-$hVDR_{gem}$ in response to 100 nM $1,25(OH)_2D_3$ (Figure 2A). Consistent with these data, gemini and Gemini-72 similarly induce the transcriptional activities of Gal4-zVDR and Gal4-$zVDR_{gem}$, whereas $1,25(OH)_2D_3$ only induces the transcriptional activity of Gal4-zVDR (Figure S5). Ligand-induced transcriptional activities were also determined in MCF-7 human breast cancer cells transiently transfected with expression vectors encoding the full-length hVDR and $hVDR_{gem}$, and a luciferase reporter plasmid encompassing the promoter region of *hCYP24A1*, a well-characterized VDR target gene (Meyer et al., 2007). Both $1,25(OH)_2D_3$ and gemini efficiently induce the transcriptional activity of hVDR (EC_{50} of 0.97 nM and 0.06 nM for $1,25(OH)_2D_3$ and gemini, respectively). While VDR_{gem} transcriptional activity is only induced by supra physiological concentrations of $1,25(OH)_2D_3$ ($\geq$1 μM), the EC_{50} of VDR_{gem} for gemini is 18.3 nM (Figure 2B). Taken together, our results show that VDR ligand binding and transcriptional activity are strongly impaired by substitution of the second VDR helix 7 N-terminal Leu to His in the presence of $1,25(OH)_2D_3$, but not of the gemini analogs.

Generation and Characterization of Mice Expressing VDR_{gem}

To analyze VDR_{gem} activity in vivo, we generated mice in which VDR Leu304 (the homolog of hVDR Leu309 and zVDR Leu337) is substituted by a His, via homologous recombination in ES cell (Figures S6A and S6B). VDR_{gem} mice, in which both VDR alleles encode the VDR His304 mutant protein, are viable but growth retarded after weaning when chow fed (Figures 3A, 3B, 5A, and 5B). They exhibit skeletal defects, including short and thick ribs, short vertebrae, reduced length of the humerus, femur and ilium, and enlargement of the humeral and femoral heads as well as of the tibial plateau (Figures 3C and 3D). At 16 weeks, bone area, bone mineral content, and bone mineral density are 30%, 35%, and 20% lower in VDR_{gem} mice than in WT

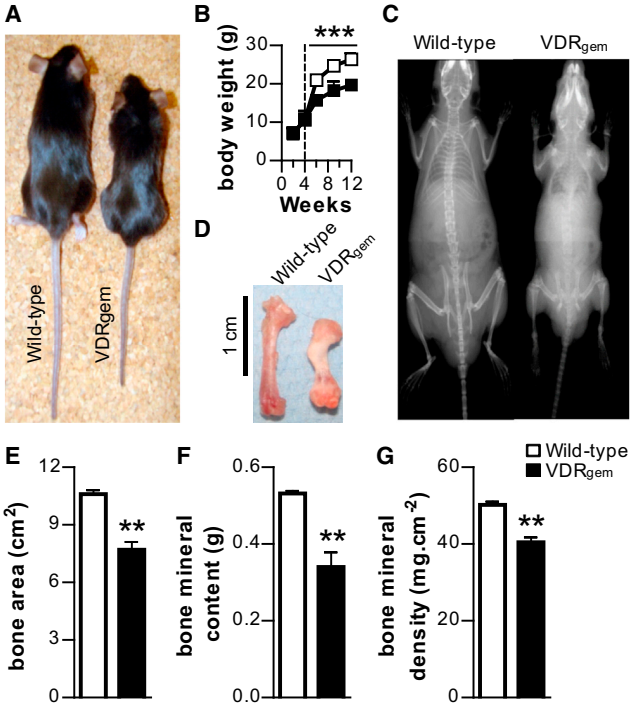

Figure 3. Phenotypic Analyses of VDR_{gem} Mice

(A) Representative picture of a 16-week-old VDR_{gem} mouse (right) and a control littermate (left).

(B) Body weight of VDR_{gem} mice (black square) and control littermates (white square) at the indicated age (n = 6). The dashed line represents weaning time.

(C and D) X-ray analysis (C) and picture (D) of a femur of a representative 16-week-old male VDR_{gem} mouse and a sex-matched control littermate.

(E–G) Bone area (E), bone mineral content (F), and bone mineral density (G) of 16-week-old male VDR_{gem} and sex-matched control littermates analyzed by dual-energy x-ray analysis scan (n = 3). Bars represent the mean ± SEM. ***p < 0.001.

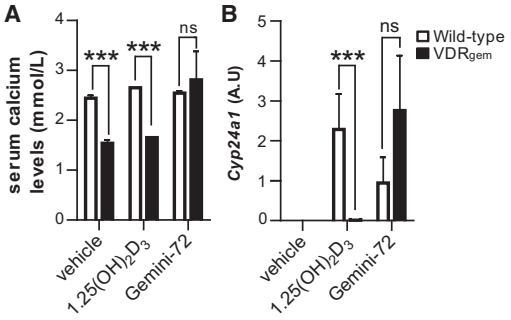

Figure 4. Serum Calcium and Duodenal *Cyp24a1* Transcript Levels in VDR_{gem} Mice after VDR Agonist Administration

(A and B) Quantification of serum calcium levels (A) and duodenal $1,25(OH)_2D_3$-24 hydroxylase (*Cyp24A1*) transcript levels (B) of 16-week-old VDR_{gem} (black bars) and control littermates (white bars) subjected to oral administration every second day of vehicle (oil), 0.3 μg/kg $1,25(OH)_2D_3$ or Gemini-72 for 3 weeks, and 3 μg/kg $1,25(OH)_2D_3$ or Gemini-72 6 hr before sacrifice. Bars represent the mean ± SEM (n = 3). ***p < 0.001. ns, not significant.

littermates, respectively (Figures 3E and 3G), and serum calcium levels are decreased by 30% (Figure 4A). However, in contrast to VDR null mice, VDR_{gem} mice do not develop alopecia even at 1 year of age (Figures 3A and 5A; data not shown). These results indicate that VDR_{gem} exhibits the typical hallmarks of $1,25(OH)_2D_3$ deficiency.

To determine whether gemini ligands induce VDR_{gem} activity in vivo, we first evaluated serum calcium levels in VDR_{gem} mice to which Gemini-72 was administered every second day at 0.3 μg/kg for 3 weeks. Such treatment does not induce hypercalcemia in WT mice, but restores serum calcium levels in VDR_{gem} mice (Figure 4A), demonstrating that VDR-dependent calcium homeostasis is normalized by Gemini-72 in these mutant mice. In contrast, $1,25(OH)_2D_3$ administration at similar doses does not increase calcium levels in VDR_{gem} mice. We next determined the transcript levels of *Cyp24a1* in the duodenum 6 hr after ligand treatment. $1,25(OH)_2D_3$ strongly induces *Cyp24a1* transcript levels in WT mice, in agreement with previous results (Meyer et al., 2007), but not in VDR_{gem} mice (Figure 4B). In contrast, Gemini-72 induces these transcript levels in both VDR_{gem} mice and control littermates. Thus, these results demonstrate that administration of Gemini-72 induces VDR_{gem} transcriptional activity and restores mineral ion homeostasis in VDR_{gem} mice.

Mineral Ion and Bone Homeostasis Is More Impaired in VDR_{gem} Than in VDR Null Mice

Whereas the body weight of VDR_{gem} mice is similar to that of WT mice and VDR null mice at weaning, it is reduced by 20% in 6-week-old VDR_{gem} and VDR null mice when chow fed. In contrast, at 10 weeks of age, while the body weight of VDR null mice is similar to that of WT mice, that of VDR_{gem} mice is decreased by 22% (Figures 5A and 5B). At this age, the body length of VDR null mice and VDR_{gem} mice is reduced by 10% and 20% compared with that of age-matched WT, respectively (Figure 5C). Moreover, the femur length is more decreased in VDR_{gem} mice than in VDR null mice (Figures 5D and 5E). In addition, hypocalcemia and hypophosphatemia are more severe in 10-week-old VDR_{gem} mice than in age-matched VDR null mice, and serum alkaline phosphatase activity is 3.2-fold more increased in VDR_{gem} mice than in VDR null mice (Figures 5F–5H). Finally, at 16 weeks, bone mineral density is 2-fold more decreased in VDR_{gem} mice than in VDR null mice (Figure 5I). Thus, mineral ion and bone homeostasis are more impaired in VDR_{gem} mice than in VDR null mice.

As duodenal VDR regulates mineral ion homeostasis (Xue and Fleet, 2009), duodenal transcriptomic analyses of 10-week-old WT, VDR_{gem}, and VDR null mice were performed, and statistically significantly deregulated transcripts with a fold change of >1.2 or <0.8 relative to WT were considered. Whereas the transcript levels of 322 genes are decreased in VDR_{gem} duodenum (Figure 6A, left), only 141 genes are downregulated in VDR null mice (Figure 6B, left). Gene ontology analysis with DAVID software revealed that among the top 100 downregulated genes in VDR_{gem} mice (Figure 6C), 38% are involved in mineral ion homeostasis (Figure 6D). In contrast, 562 genes are upregulated in VDR null mice (Figure 6B, right) and only 140 in VDR_{gem} mice (Figure 6A, right). Among the top 100 upregulated genes in duodenum of VDR_{gem} mice

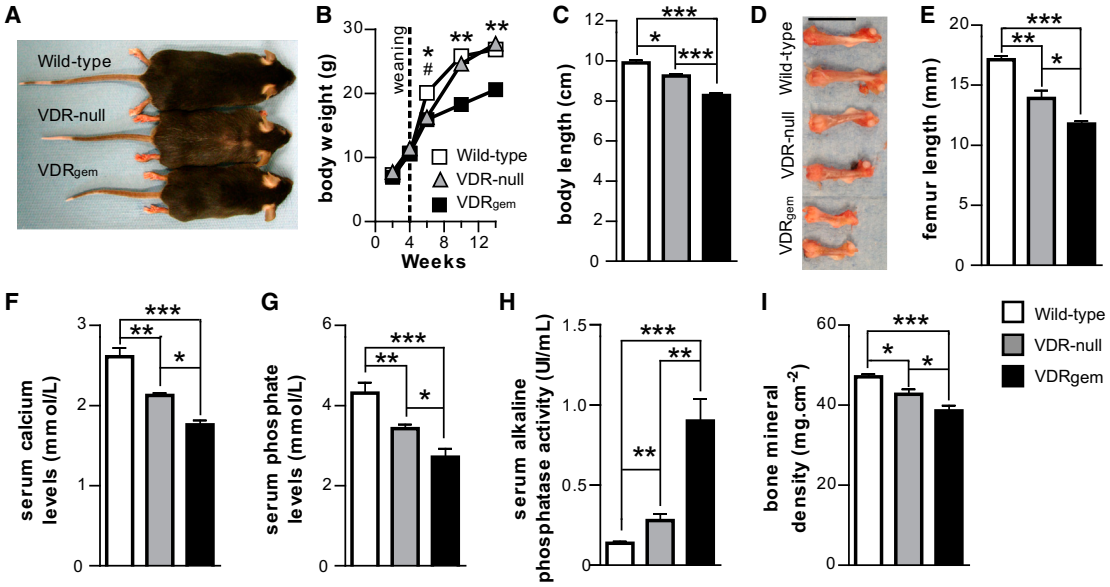

Figure 5. Phenotypic Comparison of VDR Null and VDR_{gem} Mice

(A) Representative picture of a 10-week-old WT, VDR_{gem}, and VDR null mouse. Note that at this age VDR null mice only exhibit slight alopecia, which is complete at around 5 months of age, whereas no sign of alopecia are seen in VDR_{gem} mice at any age.

(B) Body weight of VDR_{gem} mice (black square), VDR null mice (gray triangle), and control littermates (white square) at the indicated age. *p < 0.05, **p < 0.01 VDR_{gem} versus WT; #p < 0.05 VDR null versus WT. The dash line represents weaning time.

(C–G) Body length (C), representative picture of femurs (D), femur length (E), serum calcium (F), and phosphate (G) levels, serum alkaline phosphatase activity (H), and bone mineral density (I) at 10-week-old (C–H) or 16-week-old (I) WT (white bars), VDR null (gray bars), and VDR_{gem} (black bars) mice. Bars represent the mean ± SEM (n = 5). *p < 0.05, **p < 0.01, ***p < 0.001. Scale bar in (D) equals 1 cm.

(Figure 6E), 41% are involved in inflammatory and defense responses and 14% in mineral ion homeostasis (Figure 6F). Thus, these results show that the transcriptional program is differentially altered in duodenum of VDR_{gem} and VDR null mice, with 2-fold more downregulated genes in VDR_{gem} mice than in VDR null mice and 3-fold more upregulated genes in VDR null mice than in VDR_{gem} mice. Interestingly, overall, only 20 genes are upregulated, and 60 genes are downregulated in the duodenum of both VDR_{gem} and VDR null mice. Among these 60 genes, the transcript levels of 35 are more decreased in VDR_{gem} than in VDR null mice, whereas the others are similarly downregulated in both mice. As VDR_{gem} and VDR transcript levels are similar in the duodenum of VDR_{gem} mice and control littermates, and that VDR_{gem} protein levels are slightly reduced (Figures S7A and S7B), decreased gene expression in VDR_{gem} mice does not result from squelching of other transcriptional regulators by overexpression of mutant VDR.

Duodenal transcript levels of transient receptor potential cation channel, subfamily V, member 6 (*Trpv6*), which encode a protein involved in duodenal calcium absorption (Lieben and Carmeliet, 2013a), quantified by RT-QPCR, are 7.5-fold lower in VDR_{gem} mice than in control littermates, whereas those of VDR null mice are only decreased by 2-fold without reaching statistical significance (Figure 7A). Moreover, the transcript levels of solute carrier family 30 member 10 (*slc30a10*) that encodes a protein of unknown function in mice are similar in WT and VDR null mice, but are decreased by 3-fold in VDR_{gem} mice (Figure 7B). Finally, duodenal transcript levels of the VDR target gene *Cyp24a1* are reduced in both VDR null and VDR_{gem} mice, but are 5-fold lower in the latter (Figure 7C).

In agreement with previous results, chromatin immunoprecipitation with an antibody directed against VDR shows that WT VDR binds to 3′ region of *Cyp24a1* encompassing a VDRE (Meyer et al., 2010). Moreover, the same genomic region is immunoprecipitated in VDR_{gem} mice, whereas no binding is detected in VDR null mice (Figure S7C). Thus, our results show that unliganded VDR_{gem} binds VDREs and represses VDR target genes.

While administration of a supraphysiological bolus of $1,25(OH)_2D_3$ or Gemini-72 (10-fold maximal tolerated dose) for 6 hr increases the transcript levels of *Trpv6, Slc30a10*, and *Cyp24a1* in WT mice, only Gemini-72 induces their levels in VDR_{gem} mice. In contrast, the expression of these genes is not induced by these ligands in VDR null mice (Figures 7D–7F). Taken together, our results show that VDR_{gem} represses the expression of known and putative VDR target genes in the duodenum and that their expression is induced upon Gemini-72 administration, but not by $1,25(OH)_2D_3$, even at supraphysiological levels.

DISCUSSION

We previously showed that gemini ligands induce specific conformational changes in the VDR LBD by reorientation of the second N-terminal Leu of helix 7, which opens a pocket that

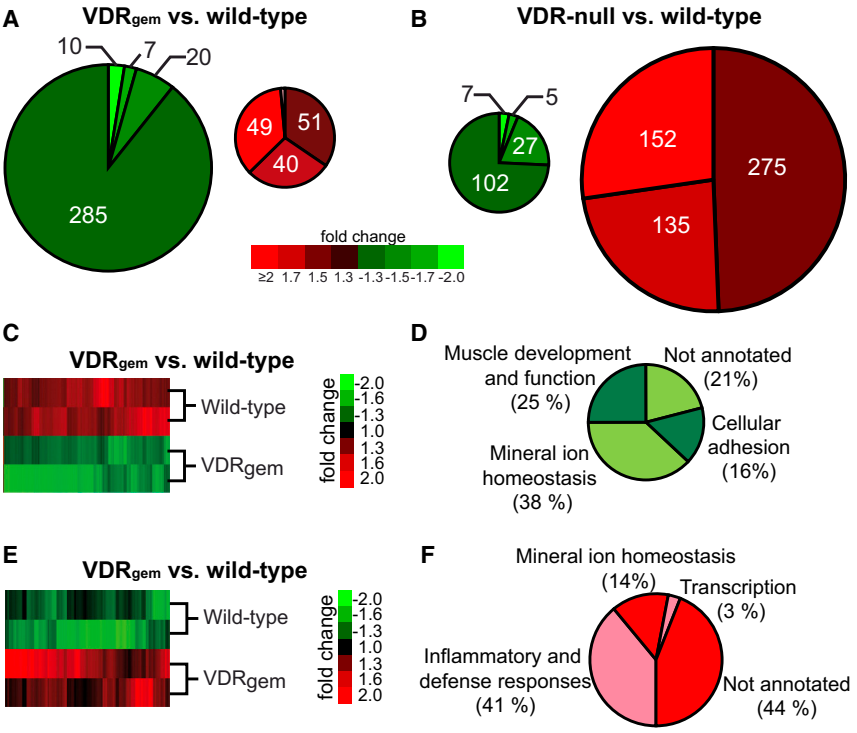

Figure 6. Transcriptomic Analysis of Duodenum from WT, VDR Null, and VDR_{gem} Mice

(A and B) Pie charts illustrating the number of downregulated (A and B, left) and upregulated (A and B, right) genes in the duodenum of 10-week-old VDR_{gem} (A) and VDR null (B) mice relative to aged matched WT mice.

(C–F) Heat map of the transcript levels of the 100 top downregulated genes (C) and the 100 top upregulated genes (E) in duodenum of 10-week-old VDR_{gem} mice relative to WT littermates and the corresponding pie charts of genome ontology annotation (D and F).

accommodates the additional side chain of such ligands (Ciesielski et al., 2007; Huet et al., 2011). The work reported here shows that substitution of this Leu to His in human or mouse VDR impairs $1,25(OH)_2D_3$, but not gemini ligand binding. VDR_{gem} elicits this discrimination by disturbing the hydrogen bond networks that anchor the natural ligand. The phenotypic features of VDR_{gem} mice expressing mVDRLeu304His are reminiscent of those of vitamin D deficiency, including hypocalcemia, rickets, and osteomalacia (Bouillon et al., 2008; Dardenne et al., 2001; Erben et al., 2002; Panda et al., 2001; Yoshizawa et al., 1997).

Numerous VDR point mutations were identified in HVDRR human patients. Those that impair DNA binding, whether located in the first or second zinc finger of the VDR DBD or in the LBD, have been shown to induce bone defects and alopecia. Patients with mutations in the VDR LBD that inhibit RXR heterodimerization, and thus strongly impair DNA binding, present alopecia, whereas those with mutations that affect $1,25(OH)_2D_3$ binding without impairing DNA binding exhibit milder bone defects, but no alopecia (Feldman and Malloy, 2014). Abnormalities resulting from mutations in the VDR LBD that selectively decrease the affinity for $1,25(OH)_2D_3$ are partially overcome by increased $1,25(OH)_2D_3$ levels in HVDRR patients (Bouillon et al., 2008; Marx et al., 1986). In contrast, a recent study has shown that alopecia, but not bone defects and mineral homeostasis, is rescued in VDR null mice by transgenic expression of a human LBD point-mutated VDR (VDR^{L233S}), unable to bind $1,25(OH)_2D_3$ (Lee et al., 2014). Interestingly, their data indicate that bone defects might be more severe in mice expressing the highest VDR^{L233S} levels. Here we show that VDR_{gem} mice, which express a VDR mutant that does not bind $1,25(OH)_2D_3$ even at supraphysiological concentrations, exhibit more impaired mineral ion and bone homeostasis than VDR null mice, but no alopecia. Thus, bone defects and mineral ion homeostasis deregulation might be more severe in patients expressing WT levels of ligand-binding deficient VDR than in those with VDR mutations impairing DNA binding, even though they do not develop alopecia.

Our duodenal transcriptomic data show that many more genes are downregulated in VDR_{gem} mice than in VDR null mice, including several known to be involved in mineral ion homeostasis. Moreover, gene downregulation is generally stronger in VDR_{gem} mice than in VDR null mice. As VDR_{gem} binds to VDREs and as unliganded VDR, thyroid hormone receptors (TRs), and retinoic acid receptors (RARs) have been shown to recruit transcriptional repressors, our results strongly support that VDR, like TR and RAR (Chambon, 2005; Perissi and Rosenfeld, 2005), represses target gene expression in its apo form.

Since treatment with gemini, but not $1,25(OH)_2D_3$, induces the expression of VDR target genes in the intestine of VDR_{gem} mice and normalizes serum calcium levels, these mice provide a valuable animal model to temporally control VDR activity and thus to further characterize in vivo receptor-mediated signaling pathways controlled by vitamin D analogs. Comparison of VDR_{gem} mice with WT and VDR null mice, treated or not with gemini analogs, should also enlighten the molecular and cellular signaling pathways controlled by $1,25(OH)_2D_3$, as well as the origin of hypercalcemic effects.

In summary, using a multidisciplinary integrative approach combining structural biology and in vivo studies, we engineered mice in which VDR activity is selectively controlled by gemini ligands and report the functional consequence of the loss of ligand-induced VDR signaling in vivo. The possibility of inducing VDR_{gem} transcriptional activity by gemini ligands allows the characterization of the in vivo genomic activities induced by various gemini analogs and to determine their functional impact at the molecular level. Thus, further phenotypic and molecular analyses in various tissues of VDR_{gem}, VDR null and WT mice treated or not with $1,25(OH)_2D_3$ or gemini ligands should provide important insights into the signaling pathways controlled by unliganded and liganded VDR, including the identification of new genes involved in vitamin D-induced hypercalcemia.

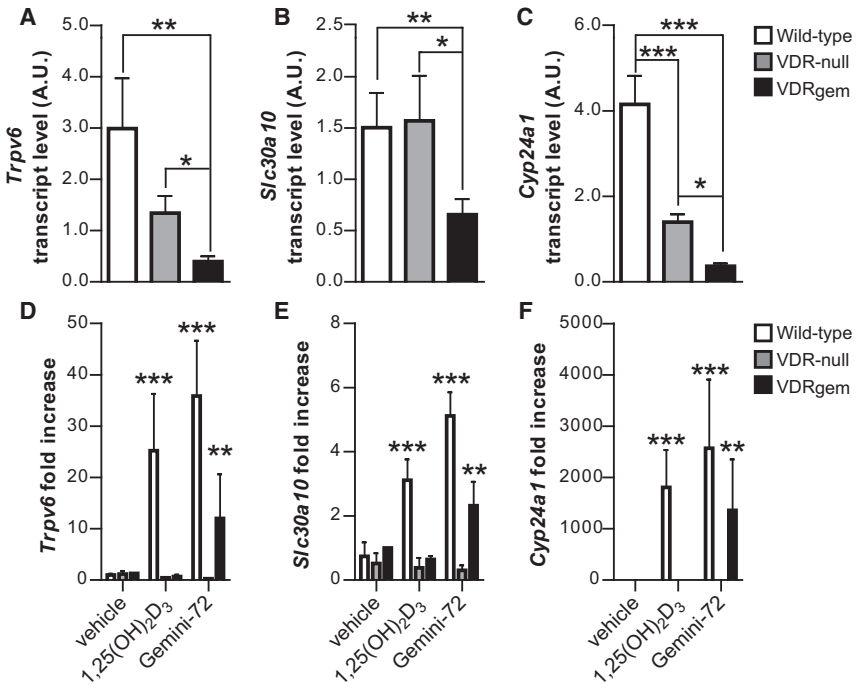

Figure 7. Transcript Levels of *Trpv6*, *Slc30a10*, and *Cyp24a1* in Duodenum of WT, VDR Null, and VDR_{gem} Mice at Basal Level and after VDR Agonist Administration

(A–C) Basal duodenal transcript levels of transient receptor potential cation channel, subfamily V, member 6 (*Trpv6*) (A), solute carrier family 30 member 10 (*Slc30a10*) (B), and $1,25(OH)_2D_3$-24 hydroxylase (*Cyp24A1*) (C), in 10-week-old WT (white bars), VDR null (gray bars), and VDR_{gem} (black bars) mice.

(D–F) Fold increase of *Trpv6* (D), *Slc30a10* (E), and *Cyp24A1* (F) duodenal transcript levels by 3 μg/kg $1,25(OH)_2D_3$ or Gemini-72 administration, relative to vehicle treatment, in 10-week-old WT (white bars), VDR null (gray bars), and VDR_{gem} (black bars) mice. Bars represent the mean ± SEM (n = 5). $^*p < 0.05$, $^{**}p < 0.01$, $^{***}p < 0.001$.

EXPERIMENTAL PROCEDURES

Vectors, Expression, and Purification

cDNAs encoding hVDRLeu309His LBD ($hVDR_{gem}$; 118–427), hVDR LBD (118–427), zVDR LBD (156–453), and zVDR Leu337His LBD ($zVDR_{gem}$; 156–453) were cloned into pET28b vector to generate N-terminal His-tag fusion proteins. Purification was carried out as previously described (Ciesielski et al., 2007; Rochel et al., 2000), including a metal affinity chromatography and a gel filtration.

Electrospray Ionization Mass Spectrometry

Prior to ESI-MS analysis, samples were desalted on Zeba Spin desalting columns (Pierce) in 200 mM ammonium acetate (pH 8.0). ESI-MS measurements were performed on an electrospray time-of-flight mass spectrometer (MicrOTOF). Purity and homogeneity of the VDR LBD proteins were verified by mass spectrometry in denaturing conditions (samples were diluted at 2 pmol/μl in a 1:1 water-acetonitrile mixture [v/v] acidified with 1% formic acid). The mass measurements of the noncovalent complexes were performed in ammonium acetate (200 mM) (pH 8.0). Samples were diluted to 8 pmol/μl in the previous buffer and continuously infused into the ESI ion source at a flow rate of 3 μl/min through a Harvard syringe pump (Harvard Apparatus model 11). A careful optimization of the interface parameters was performed to obtain the best sensitivity and spectrum quality without affecting the noncovalent complexes stability. In particular, the capillary exit ranged from 60 to 150 V with a vacuum interface pressure of 2.3 mbar and was set to 80 V. For ligand-interaction analysis, ligands were added to the proteins in a 5-fold molar excess.

Fluorescence Anisotropy

Anisotropy titrations were carried out by adding increasing concentrations of $zVDR_{gem}$ LBD complexes saturated with $1,25(OH)_2D_3$ or gemini, to a fixed concentration of tetramethylrhodamine-SRC-1 (RHKILHRLLQEGSPS) peptide (F-SRC-P). Details of the experiments and data analysis are described in the Supplemental Information and Figure S4.

Transactivation Assays

Human breast cancer MCF-7 and HEK293 EBNA cells were seeded into 24-well plates (10^5 cells per well) and grown overnight in phenol red-free DMEM supplemented with 10% charcoal-treated fetal bovine serum (FCS), 5% gentamicin, and 0.6 μg/ml insulin. Plasmid DNA containing liposomes were formed by incubating 25 ng of the expression plasmid pXJ440-Gal4 DBD-VDR LBD (zVDR [154–453] and hVDR [118–427]), 250 ng of the reporter plasmid 5x17m-TATA-*luciferase*, 50 ng of the pCH110-β-galactosidase vector (used as an internal control to normalize variation in transfection) with the transfection reagent jetPEI (Polyplus Transfection) according to the manufacturer's instructions. Transactivation assays were also performed with full-length hVDR (1–427) subcloned into the T7/SV40 promoter-driven pSG5 expression vector (Stratagene). The DNA segment of the proximal promoter region (−414 to −64) of the human *CYP24a1* gene was fused with the thymidine kinase promoter driving the firefly *luciferase* reporter gene. Plasmid DNA containing liposomes were formed by incubating 40 ng of an expression vector encoding hVDR, 100 ng of reporter plasmid, and 10 ng pEGF-C2 with Fugene 6 (Roche Diagnostics) transfection reagent for 15 min at room temperature according to the recommendation of the manufacturer. Four hours after transfections, cells were washed with freshly prepared PBS. $1,25(OH)_2D_3$, gemini, Gemini-72 ligands or solvent (DMSO) were added to the cells in phenol red-free DMEM, supplemented with 10% FCS. Twenty-four hours after the onset of stimulation, cells were washed in PBS and treated with 100 μl of reporter gene lysis buffer (Roche Diagnostics). Lysates were assayed for luciferase activity as recommended by the supplier (Perkin-Elmer). Luciferase activities were normalized to β-galactosidase or GFP expression. Data represent one triplicate.

Mammalian Two-Hybrid Assay

The Gal4 DBD in cloning vector pM and the activation-domain cloning vector pVP16 are part of the Mammalian Matchmaker Two-Hybrid Assay kit (BD Biosciences Clontech). The expression vectors for the full-length hVDR fused to VP16 (pVPVDR), the Gal4 DBD-SRC-1 NRID (pSG424-SRC-1; 570-782) and Gal4 DBD-Drip205 NRID (pM-DRIP205; 510-787) and the reporter plasmid pG5-LUC have been described previously (Eelen et al., 2005). $pVPVDR_{gem}$ was constructed by introducing the mutation in the pVPVDR by PCR using the primers that contain the mutation. HEK293 EBNA cells were plated into 24-well plates at 10^5 cells per well and grown overnight in DMEM supplemented with 10% charcoal-treated FCS and 40 μg/ml gentamycin. Details of the transfections and data analysis are given in the Supplemental Information and Figure S4.

Crystal Structures Determination

Ligands and SRC-2 (TIF-2) coactivator peptide (686- KHKILHRLLQDSS-698) were added to $zVDR_{gem}$ in a 3-fold excess to saturate the receptors. Crystallization of the $zVDR_{gem}$ complexes, diffraction data collection, and structure

refinement were obtained as described (Huet et al., 2011). Crystallographic data are summarized in Table S2.

Generation of VDR_{gem} Mice

A targeting vector, encompassing VDR exons (E) 8 to 10 in which the CTG codon encoding mouse VDR Leu304 was mutated to CAG encoding a His, and containing a LoxP flanked cassette encoding the neomycin resistance gene located in the intron between E9 and E10, was generated by PCR according to standard procedures (Duteil et al., 2010) (Figure S6). Embryonic stem cells bearing one targeted allele were identified by PCR and Southern blotting and injected into blastocystes to generate mice bearing one targeted allele, which were bred with CMV-Cre mice (Dupé et al., 1997) to excise the LoxP flanked neomycin resistance gene, and generate VDR_{gem}/+ mice bearing one VDR_{gem} allele and one VDR WT allele (Figure S6). VDR_{gem} mice, bearing two VDR_{gem} alleles, and WT littermates were generated by intercrossing VDR_{gem}/+ mice.

Mice

VDR null mice, in which exon 2 that contains the initiation codon is substituted by a neo cassette, were as described (Yoshizawa et al., 1997). Mice were maintained in a temperature- and humidity-controlled animal facility, with a 12 hr light/dark cycle and free access to water and a standard rodent chow (ref D04; 2800 kcal/kg, 9,000 mg/kg calcium and 1,000 UI/kg vitamin D_3, Usine d'Alimentation Rationelle). Animals were killed by cervical dislocation and tissues immediately collected and frozen in liquid nitrogen or processed for biochemical and histological analysis. Breeding and maintenance of mice were performed under institutional guidelines, and all experimental protocols were approved by the Animal Care and Use Committee of IGBMC.

Genotyping

VDR_{gem} and VDR null mice (Yoshizawa et al., 1997) were genotyped by PCR amplification of genomic DNA extracted from tail biopsies using the DirectPCR extraction kit (Viagen, catalog number 102-T). Primers for genotyping VDR_{gem} alleles, 5′-CAGAGACCTGCTCAGAGCCA-3′ (primer 1) and 5′-CTATGAAT GGCCTGTGGAACCCTGT-3′ (primer 3), and for VDR null alleles, 5′-CACTT GTGTAGCGCCAAGTG-3′ and 5′-TTCACAGGTCATAGCGTTGAA-3′. To verify the presence of the point mutated codon for His304, PCR products amplified with the oligonucleotides 5′-CTTGTGGGGGTTTAACCAGA-3′ (primer 2) and primer 3 were digested with Alu I.

RNA Preparation and Analysis

RNA was isolated with TRIzol Reagent (Invitrogen), and 5 μg of RNA was converted to cDNA with SuperScript II reverse transcriptase (Invitrogen, Life Technologies) and hexamers primers according to the supplier's protocol. qRT-PCR was performed using the QuantiTectTM SYBR Green PCR kit (Roche) according to the supplier's protocol. Primers were for *mCyp24a1*, 5′-GGCGGAAGATGTGAGGAATA-3′ (sense) and 5′-GCCCAGCACTTGGG TATTTA-3′ (antisense); for *mTrpv6*, 5′-CAGCAGAAGAGGATCTGGGAAT-3′ (sense) and 5′-CTCTGGTGCACCTCACATCC-3′; for *mSlc30a10*, 5′-GGTG ATTCCCTGAACACCGA-3′ (sense) and 5′-ACGTGCAAAAGAACACCTCTG-3′ (antisense); for *mVdr,* 5′-GCCACGGGCTTCCACTTCAACG-3′ (sense) and 5′-GCCTGGCAGTGTCGCCGGTT-3′ (antisense); and for *m18 S* (used as an internal standard), 5′-AGCTCACTGGCATGGCCTTC-3′ (sense) and 5′-CGCCT GCTTCACCACCTTC-3′ (antisense).

Transcriptomic Analysis

Biotinylated single-strand cDNA targets were prepared, starting from 150 ng of total RNA, using the Ambion WT Expression Kit (catalog number 4411974) and the Affymetrix GeneChip WT Terminal Labeling Kit (catalog number 900671) according to Affymetrix recommendations. Following fragmentation and end labeling, 3 μg of cDNAs were hybridized for 16 hr at 45°C on GeneChip Mouse Gene 2.0 ST arrays (Affymetrix) interrogating 35240 RefSeq transcripts represented by approximately 27 probes spread across the full length of the transcript. The chips were washed and stained in the GeneChip Fluidics Station 450 (Affymetrix) and scanned with the GeneChip Scanner 3000 7G (Affymetrix) at a resolution of 0.7 μm. Raw data (.CEL Intensity files) were extracted from the scanned images using the Affymetrix GeneChip Command Console (AGCC), v.4.0. CEL files were further processed with Affymetrix Expression Console software v.1.3.1 to calculate probe set signal intensities using Robust Multi-array Average algorithms with default settings. The FCROS method (Dembélé and Kastner, 2014) was used to select the statistically significant list of differentially expressed genes. The error level and the fold change were set to 5% and 1.2%, respectively.

Chromatin Immunoprecipitation

Nuclei of duodenum from 10-week-old mice were purified and fixed 5 min in PBS containing 1% formaldehyde and processed as described (Surjit et al., 2011). Chromatin was immunoprecipitated with the anti-VDR antibody D2K6W (cell signaling). Primers 5′-GGCCTGTGACTTCCCAGTTA-3′ (sens) and 5′-ACGTGGGATTTGCTCCTGTT-3′ (antisens) were used to amplify the 3′ genomic region of *Cyp24a1* encompassing a VDRE.

Protein Extraction and Analysis

Duodenum were grounded with a potter at 4°C in RIPA buffer (50 mM Tris [pH 7.5], 1% Nonident P40, 0.5% sodium deoxycholate, 0.1% SDS, 150 mM NaCl, 5 mM EDTA, 1 mM PMSF, and phosphatase and protease inhibitor cocktails according the manufacturer's protocol; PhosphoStop and Complete-Mini EDTA free; Roche). Homogenates (50 μg of protein) were electrophoresed on polyacrylamide gels. Proteins were electroblotted to nitrocellulose membrane using a Trans-blot turbo transfer system (Biorad), immunodetected using primary antibodies directed against VDR (D2K6W, cell signaling) and GAPDH (MAB374, Millipore Upstate Chemicon), and revealed with secondary antibodies conjugated to horseradish peroxidase (Amersham Biosciences) using an enhanced chemiluminescence detection system (ECLplus, GE Healthcare) and an ImageQuant LAS 4000 biomolecular imager (GE Healthcare).

Blood Sample Collection and Analysis

Blood for serum analysis was collected by retro-orbital puncture, and sera were prepared as described (Laverny et al., 2010). Calcium and phosphate levels and alkaline phosphatase activity were determined as described (Champy et al., 2004) and outlined on the EMPReSS website (http://www.empress.har.mrc.ac.uk).

Duel-Energy X-ray Analysis

Bone mineral density and bone mineral content were determined by dual-energy x-ray analysis on an ultrahigh-resolution densitometer PIXImus (GE Medical Systems) (Picardi et al., 2002).

ACCESSION NUMBERS

Coordinates and structure factors are deposited into the Protein Data Bank with accession numbers 4RUJ for VDR_{gem}-1,25$(OH)_2D_3$, 4RUO for VDR_{gem}-gemini, and 4RUP for VDR_{gem}-Gemini72.

SUPPLEMENTAL INFORMATION

Supplemental Information includes Supplemental Experimental Procedures, seven figures, and three tables and can be found with this article online at http://dx.doi.org/10.1016/j.celrep.2014.12.045.

AUTHOR CONTRIBUTIONS

T.H. purified, crystallized, collected, processed, and refined x-ray data and performed functional assays. F.C., F.M., and A.Y.B. performed cellular functional assays. N.P. performed ESI-MS analyses. G.L. and T.G.R performed in vivo studies. T.H., G.L., D. Metzger, D. Moras, and N.R. designed the study and analyzed data. T.H., G.L., P.A., D. Metzger, D. Moras, and N.R. wrote the paper.

ACKNOWLEDGMENTS

We thank M. Uskokovic and H. Maehr for providing the gemini and Gemini-72 ligands and S. Kato for VDR-null mice. We thank L. Verlinden and A. Verstuyf for the plasmids for the two-hybrid assay. We also thank M. Mark and Y. Sato

for discussions, P. Eberling for the peptide synthesis, the IGBMC microarray and sequencing platform for data generation and bioinformatics support, the staff of the mouse, biochemistry and genetic engineering facilities from ICS and IGBMC for technical assistance, and the staff of the beamline at the ESRF for the experimental assistance during data collection. The project was supported by the Centre National de la Recherche Scientifique, the Institut National de la Santé et de la Recherche Médicale, the Agence Nationale de la Recherche (ANR-13-BSV8-0024-01), the Fondation ARC pour la Recherche sur le Cancer, Instruct, part of the European Strategy Forum on Research Infrastructures, and the French Infrastructure for Integrated Structural Biology (ANR-10-INSB-05-01) and by French state funds through the Agence Nationale de la Recherche ANR-10-LABX-0030-INRT under the frame programme Investissements d'Avenir labelled ANR-10-IDEX-0002-02.

Received: August 14, 2014
Revised: November 8, 2014
Accepted: December 2, 2014
Published: January 22, 2015

REFERENCES

Adorini, L., Amuchastegui, S., Corsiero, E., Laverny, G., Le Meur, T., and Penna, G. (2007). Vitamin D receptor agonists as anti-inflammatory agents. Expert Rev. Clin. Immunol. *3*, 477–489.

Bouillon, R., and Suda, T. (2014). Vitamin D: calcium and bone homeostasis during evolution. Bonekey Rep. *3*, 480.

Bouillon, R., Carmeliet, G., Verlinden, L., van Etten, E., Verstuyf, A., Luderer, H.F., Lieben, L., Mathieu, C., and Demay, M. (2008). Vitamin D and human health: lessons from vitamin D receptor null mice. Endocr. Rev. *29*, 726–776.

Chambon, P. (2005). The nuclear receptor superfamily: a personal retrospect on the first two decades. Mol. Endocrinol. *19*, 1418–1428.

Champy, M.F., Selloum, M., Piard, L., Zeitler, V., Caradec, C., Chambon, P., and Auwerx, J. (2004). Mouse functional genomics requires standardization of mouse handling and housing conditions. Mamm. Genome *15*, 768–783.

Chen, C.H., Sakai, Y., and Demay, M.B. (2001). Targeting expression of the human vitamin D receptor to the keratinocytes of vitamin D receptor null mice prevents alopecia. Endocrinology *142*, 5386–5389.

Ciesielski, F., Rochel, N., and Moras, D. (2007). Adaptability of the Vitamin D nuclear receptor to the synthetic ligand Gemini: remodelling the LBP with one side chain rotation. J. Steroid Biochem. Mol. Biol. *103*, 235–242.

Dardenne, O., Prud'homme, J., Arabian, A., Glorieux, F.H., and St-Arnaud, R. (2001). Targeted inactivation of the 25-hydroxyvitamin D(3)-1(alpha)-hydroxylase gene (CYP27B1) creates an animal model of pseudovitamin D-deficiency rickets. Endocrinology *142*, 3135–3141.

Dardenne, O., Prudhomme, J., Hacking, S.A., Glorieux, F.H., and St-Arnaud, R. (2003). Rescue of the pseudo-vitamin D deficiency rickets phenotype of CYP27B1-deficient mice by treatment with 1,25-dihydroxyvitamin D3: biochemical, histomorphometric, and biomechanical analyses. J. Bone Miner. Res. *18*, 637–643.

Dembélé, D., and Kastner, P. (2014). Fold change rank ordering statistics: a new method for detecting differentially expressed genes. BMC Bioinformatics *15*, 14.

Dupé, V., Davenne, M., Brocard, J., Dollé, P., Mark, M., Dierich, A., Chambon, P., and Rijli, F.M. (1997). In vivo functional analysis of the Hoxa-1 3′ retinoic acid response element (3′RARE). Development *124*, 399–410.

Duteil, D., Chambon, C., Ali, F., Malivindi, R., Zoll, J., Kato, S., Geny, B., Chambon, P., and Metzger, D. (2010). The transcriptional coregulators TIF2 and SRC-1 regulate energy homeostasis by modulating mitochondrial respiration in skeletal muscles. Cell Metab. *12*, 496–508.

Eelen, G., Verlinden, L., Rochel, N., Claessens, F., De Clercq, P., Vandewalle, M., Tocchini-Valentini, G., Moras, D., Bouillon, R., and Verstuyf, A. (2005). Superagonistic action of 14-epi-analogs of 1,25-dihydroxyvitamin D explained by vitamin D receptor-coactivator interaction. Mol. Pharmacol. *67*, 1566–1573.

Erben, R.G., Soegiarto, D.W., Weber, K., Zeitz, U., Lieberherr, M., Gniadecki, R., Möller, G., Adamski, J., and Balling, R. (2002). Deletion of deoxyribonucleic acid binding domain of the vitamin D receptor abrogates genomic and nongenomic functions of vitamin D. Mol. Endocrinol. *16*, 1524–1537.

Feldman, D., and Malloy, P.J. (2014). Mutations in the vitamin D receptor and hereditary vitamin D-resistant rickets. Bonekey Rep. *3*, 510.

Huet, T., Maehr, H., Lee, H.J., Uskokovic, M.R., Suh, N., Moras, D., and Rochel, N. (2011). Structure-function study of gemini derivatives with two different side chains at C-20, Gemini-0072 and Gemini-0097. Medchemcomm *2*, 424–429.

Laverny, G., Penna, G., Uskokovic, M., Marczak, S., Maehr, H., Jankowski, P., Ceailles, C., Vouros, P., Smith, B., Robinson, M., et al. (2009). Synthesis and anti-inflammatory properties of 1alpha,25-dihydroxy-16-ene-20-cyclopropyl-24-oxo-vitamin D3, a hypocalcemic, stable metabolite of 1alpha,25-dihydroxy-16-ene-20-cyclopropyl-vitamin D3. J. Med. Chem. *52*, 2204–2213.

Laverny, G., Penna, G., Vetrano, S., Correale, C., Nebuloni, M., Danese, S., and Adorini, L. (2010). Efficacy of a potent and safe vitamin D receptor agonist for the treatment of inflammatory bowel disease. Immunol. Lett. *131*, 49–58.

Lee, H.J., Paul, S., Atalla, N., Thomas, P.E., Lin, X., Yang, I., Buckley, B., Lu, G., Zheng, X., Lou, Y.R., et al. (2008). Gemini vitamin D analogues inhibit estrogen receptor-positive and estrogen receptor-negative mammary tumorigenesis without hypercalcemic toxicity. Cancer Prev. Res. (Phila.) *1*, 476–484.

Lee, S.M., Goellner, J.J., O'Brien, C.A., and Pike, J.W. (2014). A humanized mouse model of hereditary 1,25-dihydroxyvitamin D-resistant rickets without alopecia. Endocrinology *155*, 4137–4148.

Leyssens, C., Verlinden, L., and Verstuyf, A. (2014). The future of vitamin D analogs. Front Physiol *5*, 122.

Li, Y.C., Pirro, A.E., Amling, M., Delling, G., Baron, R., Bronson, R., and Demay, M.B. (1997). Targeted ablation of the vitamin D receptor: an animal model of vitamin D-dependent rickets type II with alopecia. Proc. Natl. Acad. Sci. USA *94*, 9831–9835.

Lieben, L., and Carmeliet, G. (2013a). The delicate balance between vitamin D, calcium and bone homeostasis: lessons learned from intestinal- and osteocyte-specific VDR null mice. J. Steroid Biochem. Mol. Biol. *136*, 102–106.

Lieben, L., and Carmeliet, G. (2013b). Vitamin D signaling in osteocytes: effects on bone and mineral homeostasis. Bone *54*, 237–243.

Lieben, L., Carmeliet, G., and Masuyama, R. (2011). Calcemic actions of vitamin D: effects on the intestine, kidney and bone. Best Pract. Res. Clin. Endocrinol. Metab. *25*, 561–572.

Lieben, L., Masuyama, R., Torrekens, S., Van Looveren, R., Schrooten, J., Baatsen, P., Lafage-Proust, M.H., Dresselaers, T., Feng, J.Q., Bonewald, L.F., et al. (2012). Normocalcemia is maintained in mice under conditions of calcium malabsorption by vitamin D-induced inhibition of bone mineralization. J. Clin. Invest. *122*, 1803–1815.

Lips, P. (2006). Vitamin D physiology. Prog. Biophys. Mol. Biol. *92*, 4–8.

Lou, Y.R., Molnár, F., Peräkylä, M., Qiao, S., Kalueff, A.V., St-Arnaud, R., Carlberg, C., and Tuohimaa, P. (2010). 25-Hydroxyvitamin D(3) is an agonistic vitamin D receptor ligand. J. Steroid Biochem. Mol. Biol. *118*, 162–170.

Maehr, H., Uskokovic, M., Adorini, L., Penna, G., Mariani, R., Panina, P., Passini, N., Bono, E., Perego, S., Biffi, M., et al. (2007). Calcitriol derivatives with two different side chains at C-20 III. An epimeric pair of the gemini family with unprecedented antiproliferative effects on tumor cells and renin mRNA expression inhibition. J. Steroid Biochem. Mol. Biol. *103*, 277–281.

Malloy, P.J., and Feldman, D. (2011). The role of vitamin D receptor mutations in the development of alopecia. Mol. Cell. Endocrinol. *347*, 90–96.

Malloy, P.J., Tasic, V., Taha, D., Tütüncüler, F., Ying, G.S., Yin, L.K., Wang, J., and Feldman, D. (2014). Vitamin D receptor mutations in patients with hereditary 1,25-dihydroxyvitamin D-resistant rickets. Mol. Genet. Metab. *111*, 33–40.

Marx, S.J., Bliziotes, M.M., and Nanes, M. (1986). Analysis of the relation between alopecia and resistance to 1,25-dihydroxyvitamin D. Clin. Endocrinol. (Oxf.) *25*, 373–381.

Meyer, M.B., Zella, L.A., Nerenz, R.D., and Pike, J.W. (2007). Characterizing early events associated with the activation of target genes by 1,25-dihydroxyvitamin D3 in mouse kidney and intestine in vivo. J. Biol. Chem. *282*, 22344–22352.

Meyer, M.B., Goetsch, P.D., and Pike, J.W. (2010). A downstream intergenic cluster of regulatory enhancers contributes to the induction of CYP24A1 expression by 1alpha,25-dihydroxyvitamin D3. J. Biol. Chem. *285*, 15599–15610.

Panda, D.K., Miao, D., Tremblay, M.L., Sirois, J., Farookhi, R., Hendy, G.N., and Goltzman, D. (2001). Targeted ablation of the 25-hydroxyvitamin D 1alpha -hydroxylase enzyme: evidence for skeletal, reproductive, and immune dysfunction. Proc. Natl. Acad. Sci. USA *98*, 7498–7503.

Perissi, V., and Rosenfeld, M.G. (2005). Controlling nuclear receptors: the circular logic of cofactor cycles. Nat. Rev. Mol. Cell Biol. *6*, 542–554.

Picardi, M., Muretto, P., De Rosa, G., Selleri, C., De Renzo, A., Persico, M., and Rotoli, B. (2002). Color ultrasound-guided fine needle cutting biopsy for the characterization of diffuse liver damage in critical bone marrow transplanted patients. Haematologica *87*, 652–657.

Rochel, N., and Moras, D. (2006). Ligand binding domain of vitamin D receptors. Curr. Top. Med. Chem. *6*, 1229–1241.

Rochel, N., Wurtz, J.M., Mitschler, A., Klaholz, B., and Moras, D. (2000). The crystal structure of the nuclear receptor for vitamin D bound to its natural ligand. Mol. Cell *5*, 173–179.

Skorija, K., Cox, M., Sisk, J.M., Dowd, D.R., MacDonald, P.N., Thompson, C.C., and Demay, M.B. (2005). Ligand-independent actions of the vitamin D receptor maintain hair follicle homeostasis. Mol. Endocrinol. *19*, 855–862.

Surjit, M., Ganti, K.P., Mukherji, A., Ye, T., Hua, G., Metzger, D., Li, M., and Chambon, P. (2011). Widespread negative response elements mediate direct repression by agonist-liganded glucocorticoid receptor. Cell *145*, 224–241.

Xue, Y., and Fleet, J.C. (2009). Intestinal vitamin D receptor is required for normal calcium and bone metabolism in mice. Gastroenterology *136*, 1317–1327, e1–e2.

Yoshizawa, T., Handa, Y., Uematsu, Y., Takeda, S., Sekine, K., Yoshihara, Y., Kawakami, T., Arioka, K., Sato, H., Uchiyama, Y., et al. (1997). Mice lacking the vitamin D receptor exhibit impaired bone formation, uterine hypoplasia and growth retardation after weaning. Nat. Genet. *16*, 391–396.